Journal of The Electrochemical Society, **148** (8) A951-A959 (2001)
0013-4651/2001/148(8)/A951/9/$7.00 © The Electrochemical Society, Inc.

A ^{7}Li Nuclear Magnetic Resonance Study of Metal-Substituted Lithium Manganese Oxide Spinels

Michael C. Tucker,[a,*] Jeffrey A. Reimer,[a] and Elton J. Cairns[b,,z]**

[a]*Department of Chemical Engineering, University of California, Berkeley, California, USA*
[b]*Ernest Orlando Lawrence Berkeley National Laboratory, Berkeley, California, USA*

Metal-substituted spinels, $LiM_xMn_{2-x}O_4$ (M = Li, Zn, Ni, Al, Co, Cr), are synthesized with low levels of substitution by solid-state techniques and studied with ^{7}Li magic angle spinning nuclear magnetic resonance (MAS NMR). The NMR spectra are characterized by several distinct peaks, spanning a wide shift range. The shifts are interpreted in terms of the supertransferred hyperfine interaction. The as-prepared spinels show peaks in the vicinity of 510 ppm, assigned to ''normal'' lithium in a tetrahedral site surrounded by 12 manganese nearest neighbors, and 530-580 ppm, assigned to ''near-defect'' lithium in a tetrahedral site with one or more metal substituents as nearest neighbors. Upon substitution, the peak arising from normal lithium broadens and reduces in intensity, whereas the peaks arising from near-defect lithium increase in intensity. Li-, Co-, and Al-substituted spinels also give rise to a peak in the vicinity of 1700 ppm, assigned to electrochemically inactive lithium in the 16d octahedral site. NMR spectra of electrochemically cycled spinels reveal that the local environment of lithium changes upon cycling. After cycling, the normal lithium peak reduces in intensity and broadens, while the near-defect lithium peak increases in intensity. The extent of these changes is least for spinels that show robust capacity retention. It is found that damage from moisture contamination results in a shift and reduction in intensity of the peak arising from tetrahedral lithium in the spinel. In addition, a new peak at 0 ppm is observed and assigned to multiple diamagnetic, lithium-containing solid electrolyte interface species. No effects of moisture contamination are observed in the electrochemically prepared samples.
 [DOI: 10.1149/1.1383775]

Manuscript received October 11, 2000. Available electronically July 13, 2001.

The lithium manganese oxide spinel $LiMn_2O_4$, is a promising alternative to commercially available lithium rechargeable battery cathode materials based on nickel and cobalt oxides. $LiMn_2O_4$ displays a high initial capacity on the 4 V plateau, but has been plagued by an unacceptable capacity fade. It is well known that substituting mono-, di-, or trivalent metal cations for manganese improves the spinel's capacity retention, at the cost of initial capacity, due to increased average manganese oxidation state. A previous nuclear magnetic resonance (NMR) study of Li-, Co-, and Ni-substitution showed that the supertransferred hyperfine coupling constant, a measure of the Li-O-Mn bond covalency, increased with substitution.[1] This suggested that increased covalency upon substitution might be responsible for a more robust spinel, and showed that NMR is sensitive to structural factors that might directly affect electrochemical performance. More recent magic angle spinning (MAS) NMR studies have shown that NMR can distinguish chemically distinct types of lithium in the spinel structure on the basis of variations in the lithium local coordination shell arising from the presence of defects, changes in manganese oxidation state, etc.[2-4] In this study, we use ^{7}Li MAS NMR to characterize metal-substituted spinels, prepared by traditional solid-state techniques. We have chosen to study primarily compositions with low levels of substitution, which yield high capacities and are therefore industrially relevant. This characterization may provide the basis for future work attempting to elucidate the causes of spinel degradation upon electrochemical cycling, and the mechanism of capacity stabilization by metal substitution.

Experimental

Sample preparation.—$LiM_xMn_{2-x}O_4$ (M = Cr, Co, Al, Zn, Ni) were prepared from a stoichiometric mixture of Li_2CO_3 (J.T. Baker), MnO_2 (Japan Metals, CMD) and the metal oxide. The mixture was fired at 850°C in flowing oxygen for 20 h with one intermediate grinding, and then cooled at 50°C/h $Li_{1+x}Mn_{2-x}O_4$ was prepared according to the procedure in Ref. 5; $LiMn_2O_4$ (prepared as above) was mixed with the necessary amount of Li_2CO_3 and refired at 600°C; all other conditions were the same.

Sample characterization.—The spinels were characterized by X-ray diffraction (XRD) on a Siemens D5000 diffractometer using Cu $K\alpha_1$ radiation. A small amount of silicon was added to the samples as an internal standard and all peak positions used for cell parameter determination were adjusted according to the difference between the observed and calculated silicon peaks. Cell parameters were obtained using UnitCell for the Macintosh. Reproducibility of the synthesis procedure and the XRD characterization was determined by preparing and analyzing multiple batches of selected spinel compositions. Cell parameters were reproducible to 0.001 Å. Particle size distribution was measured with a Coulter LS230 laser diffraction particle size analyzer. The particle size ranged from one to 100 μm, with an average of 22 μm.

Electrochemical studies.—Electrodes were prepared by dispersing spinel, acetylene black (Shawinigan), graphite (Timcal), and poly(vinylidene flouride) (PVDF, Elf Atochem) (90:2:4:4) in *n*-methyl pyrrolidinone (NMP, Aldrich). The dispersion was cast onto stainless steel foil and dried at 150°C for 40 min, resulting in a final electrode thickness of ~250 μm. This yields sufficient material for the NMR experiment. Electrodes were punched out and dried overnight at 100°C under vacuum before being transferred to a helium-filled glove box for cell assembly. Cells were prepared by sandwiching a spinel electrode against a lithium foil with Celgard 3401 (DuPont) separator and flooded with 1 M $LiPF_6$ in ethylene carbonate/dimethyl carbonate (EC/DMC) (1:2) (EM Industries) electrolyte in a stainless steel Swagelok union. Cell cycling was performed using an Arbin battery tester. Cells were cycled between 3.3 and 4.4 V at a C/15 rate, with 30 min open circuit periods between half cycles. After cycling, all samples were returned to a nominal composition of $LiM_xMn_{2-x}O_4$ by discharging to 3.05 V and letting the current decay to less than 0.1 μA/mg. Electrochemical lithium extraction was achieved by charging to 4.4 V and letting the current decay to less than 0.1 μA/mg. After electrochemical preparation, electrode samples were washed with acetonitrile to remove excess electrolyte.

NMR studies.—NMR experiments were performed on a home-built spectrometer, with a 7 mm MAS probe (Doty Scientific) tuned to ^{7}Li frequency of 70.37 MHz. All shifts were referenced to 1 M $LiCl_{(aq)}$. A 90°-τ-180° (90° = 1 μs) pulse sequence with τ = (spinning frequency)$^{-1}$ was used to obtain the spectra shown. A recycle delay of 500 ms was used to avoid saturation of the signal.

* Electrochemical Society Student Member.
** Electrochemical Society Fellow.
z E-mail: ejcairns@lbl.gov

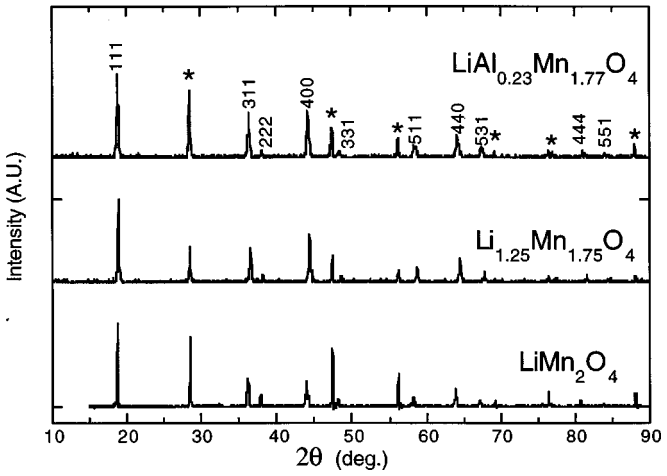

Figure 1. XRD traces for selected spinel compositions. Internal silicon standard peaks are marked with an (*).

Isotropic peaks were identified by varying the spinning speed. An inversion recovery sequence was used to measure T_1 (spin-lattice relaxation time). The spin-lattice relaxation time for $LiMn_2O_4$ was found to be 4 ms for the peak at ~500 ppm and 6-7 ms for the two smaller peaks. The spin-lattice relaxation time for $LiAl_{0.1}Mn_{1.9}O_4$ was found to be 6 ms for the peak at ~500 ppm and 4-5 ms for the two smaller peaks. T_2 (spin-spin relaxation time) was estimated by varying the delay between the 90 and 180° pulses to be integer multiples of the rotor period. Fitting the exponential decay of the echo intensity *vs.* pulse delay length yields an estimate of T_2. For example, for $LiAl_{0.1}Mn_{1.9}O_4$, this was found to be 1.5 ms for the peak at 500 ppm, and 0.9 ms for the peaks at 540 and 570 ppm. With a high spinning speed and short rotor period, we conclude that spectral distortion from these differing T_2 values will be minimal. It was found that sample magnetism has a significant effect on probe tuning and quality factor (Q). This effect was minimized so as to obtain quantitative spectra by diluting all samples with rocksalt. The spectral intensity per gram of sample varied by less than 10% over the dilution range of 20-33 wt % sample. All fresh materials were diluted to 25-28 wt % sample.

Results and Discussion

XRD traces of selected spinels are shown in Fig. 1. All samples were found to be cubic single phase (space group $Fd3m$), with the exception of heavily Al-substituted samples ($y > 0.1$) which showed traces of Al_2O_3. The variation of the lattice parameter with manganese oxidation state is shown in Fig. 2. Regardless of the substituting metal, a decrease in the lattice parameter is seen with increasing substitution (increasing manganese oxidation state). This is primarily due to a change in the average nominal manganese oxidation state, as the octahedral crystal radii of Mn(III) and Mn(IV) are 0.785 and 0.670 Å, respectively.[6] For a given manganese oxidation state, the contraction of the unit cell varies with metal substituent, roughly following the order Al > Co > Cr > Zn > Ni > Li. This is expected on the basis of the metal ions' octahedral crystal radii, Al(III):0.675, Co(III):0.685, Cr(III):0.755, Ni(II):0.83, Zn(II)0.88, and Li(I):0.9.[6] The values of the lattice parameter for $Li_{1+x}Mn_{2-x}O_4$ are in close agreement with the literature values.[5]

The room-temperature magnetic susceptibility of the spinels is shown in Fig. 3. The wide range of sample susceptibilities required dilution of the samples with a diamagnetic inert, as described above. With the exception of the Co-substituted spinels, the magnetic susceptibility is a generally increasing function of manganese oxidation state. We surmise that substitution for manganese by the cations and increased manganese oxidation state reduce the number of unpaired electrons in the sample, and therefore consider nonparamagnetic interactions in order to account for the observed trend. Previous work by Gee *et al.*,[1] has shown that the Weiss constants for Li-, Ni-, and Co-substituted spinels increase with substitution from a value of −231 K for $LiMn_2O_4$ to 48, 36, and −70 K for $Li_4Mn_5O_{12}$, $LiNi_{0.25}Mn_{1.75}O_4$, and $LiCo_{0.5}Mn_{1.5}O_4$, respectively.

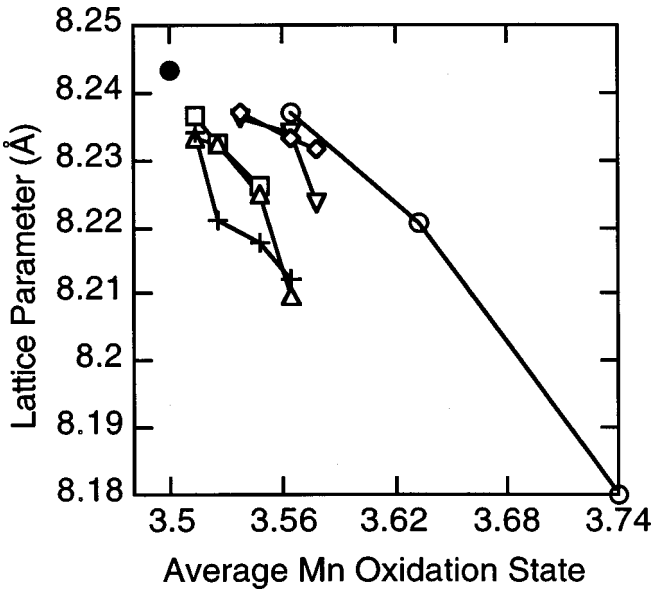

Figure 2. Lattice parameter for various spinels, $LiM_xMn_{2-x}O_4$, calculated from XRD traces. The substituting metals are labeled as (●) $LiMn_2O_4$ (○) Li, (▽) Zn, (◇) Ni, (□) Cr, (△) Co, and (+) Al.

The large negative Weiss constant for $LiMn_2O_4$ indicates significant antiferromagnetic interactions between the manganese unpaired electrons. In the simplest picture, substitution for manganese frustrates long-range antiferromagnetism, and the full paramagnetic susceptibility of the manganese cations is approached as the substitution level increases. It is unclear why the magnetic susceptibility decreases upon cobalt substitution, but the present results agree qualitatively with the results of Gee *et al.*[1]

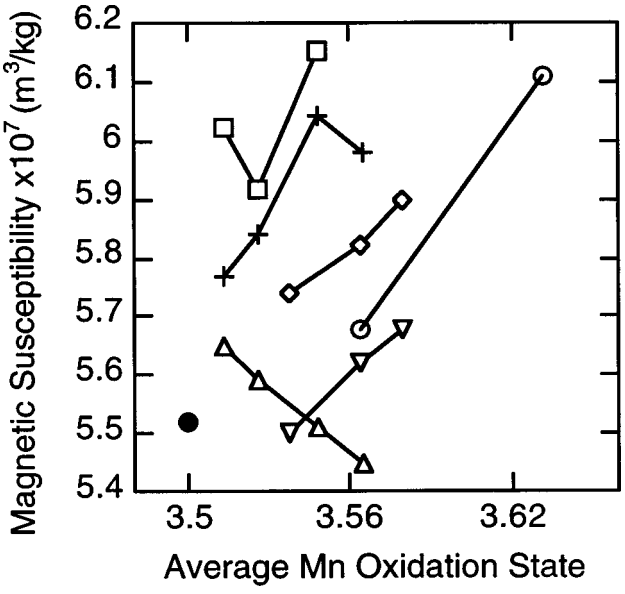

Figure 3. Magnetic susceptibility of various spinels, $LiM_xMn_{2-x}O_4$, measured with SQUID at 300 K. The substituting metals are labeled as (●) $LiMn_2O_4$ (○) Li, (▽) Zn, (◇) Ni, (□) Cr, (△) Co, and (+) Al.

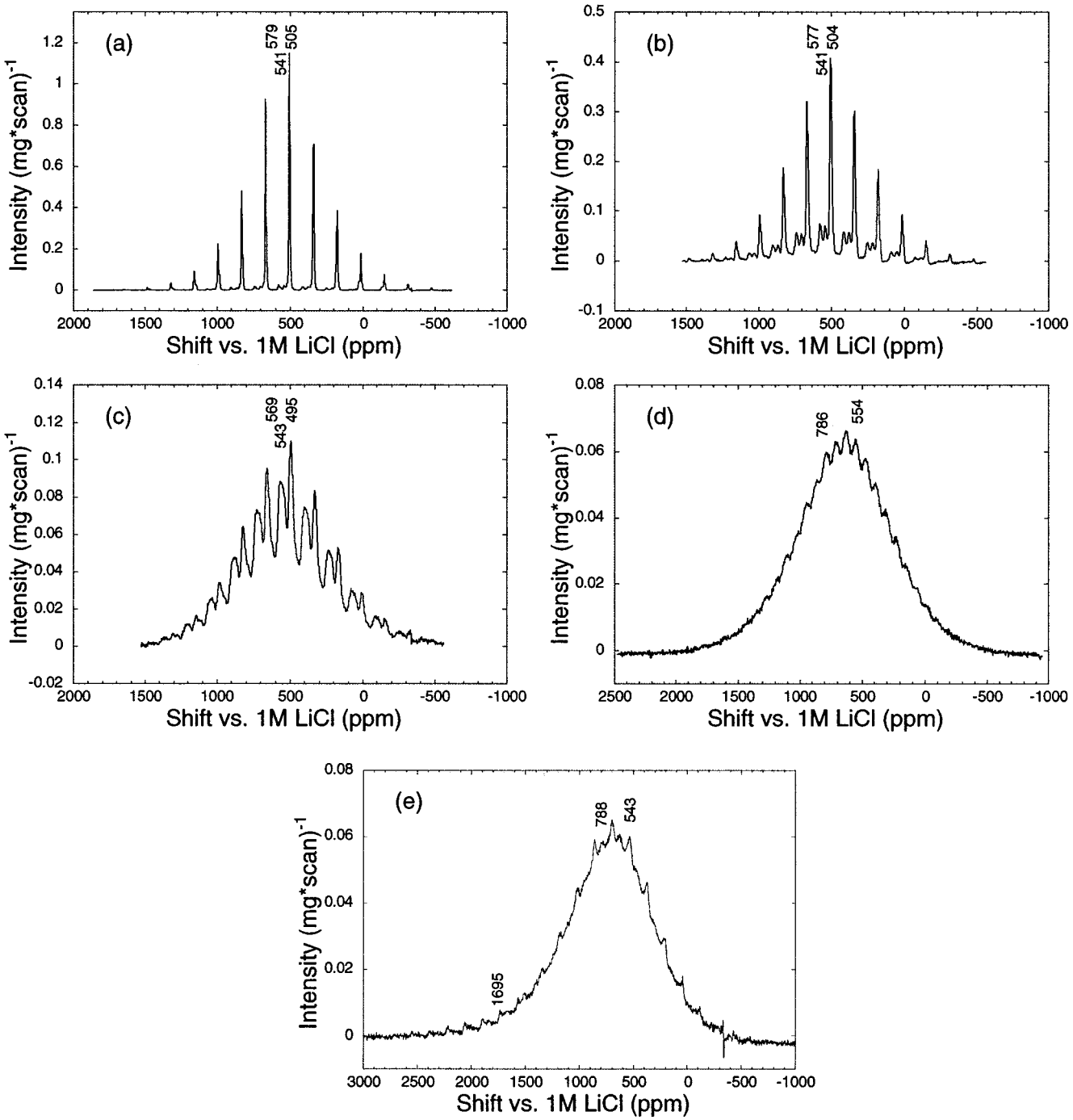

Figure 4. ^{7}Li MAS NMR spectra for as-prepared $Li_{1+x}Mn_{2-x}O_4$; x = (a) 0, (b) 0.05, (c) 0.1, (d) 0.175, (e) 0.25. Isotropic peaks are labeled.

NMR studies of as-prepared spinels.—The NMR spectra of all as-prepared compositions studied are shown in Fig. 4-10. Full spectra are shown only for representative compositions; the tetrahedral isotropic peaks are shown for all compositions. All spectra were obtained at a spinning speed of 11.5 kHz. The spin rate was not allowed to vary by more than 30 Hz over the course of a single experiment, or from sample to sample. This precaution is necessary because the isotropic shifts in these materials are highly temperature dependent,[1] and sample temperature varies with spin rate due to frictional heating. In fact, it was found that observed shifts varied by as much as 12 ppm per kHz variation in spin rate in the range 10-12 kHz. Carefully controlling the spin rate therefore allows an accurate comparison of the shifts, as well as precludes inhomogeneous line-broadening arising from temperature variations over the course of an experiment.

The ^{7}Li MAS NMR spectrum for $LiMn_2O_4$ (Fig. 4a) is characterized by a large peak at 505 ppm, and two smaller peaks at 540 and 580 ppm. These peaks have been observed previously, and can be assigned by comparison to the literature.[3] The peak at 505 ppm is assigned to tetrahedral lithium in the normal cubic (8a) lattice site, and is hereafter referred to as the normal lithium peak; the peaks at 540 and 580 ppm derive from lithium in the 8a site in close proximity to lattice defects (*i.e.*, Mn vacancy or Li-for-Mn substitution),[3] and are hereafter referred to as the near-defect lithium peaks. Previous works[1,3] have shown the supertransferred hyperfine interaction

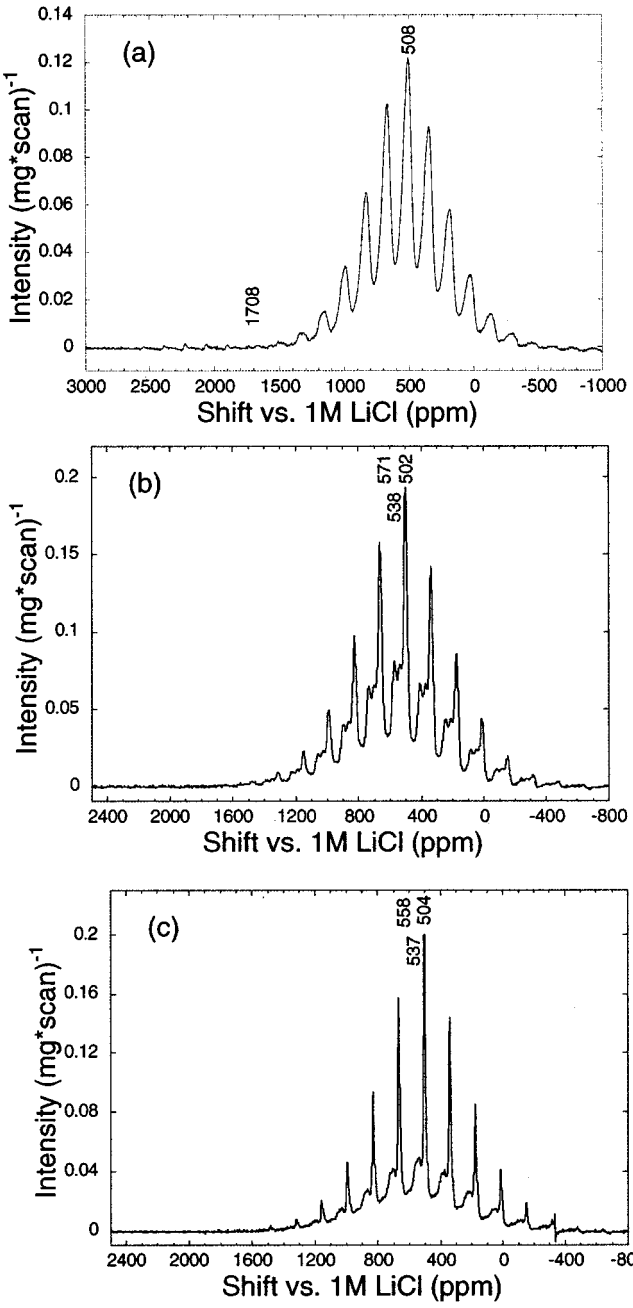

Figure 5. ^{7}Li MAS NMR spectra for representative as-prepared spinels. (a) $LiCo_{0.23}Mn_{1.77}O_4$, (b) $LiAl_{0.1}Mn_{1.9}O_4$, (c) $LiNi_{0.082}Mn_{1.918}O_4$. Isotropic peaks are labeled.

between unpaired manganese d electrons and the lithium nucleus to be the dominant shift mechanism in these materials. Transfer of transition metal t_{2g} unpaired electron density to the lithium orbitals can occur in a bent Li-O-Mn bond, resulting in a shift of the lithium resonance to higher frequency. In the case of a partially filled e_g orbital, unpaired spin density can only be transferred to the lithium orbitals in a linear Li-O-Mn arrangement, due to geometric constraints of the oxygen p-metal d orbital overlap. Such an arrangement results in a shift of the lithium resonance to lower frequency. The Li-O-Mn bond angle for tetrahedral lithium falls between the linear and bent extremes, and supertransferred hyperfine shifts arising from both t_{2g} and e_g electrons are observed. For example, the shift of tetrahedral lithium in $Li_yMn_2O_4$ moves

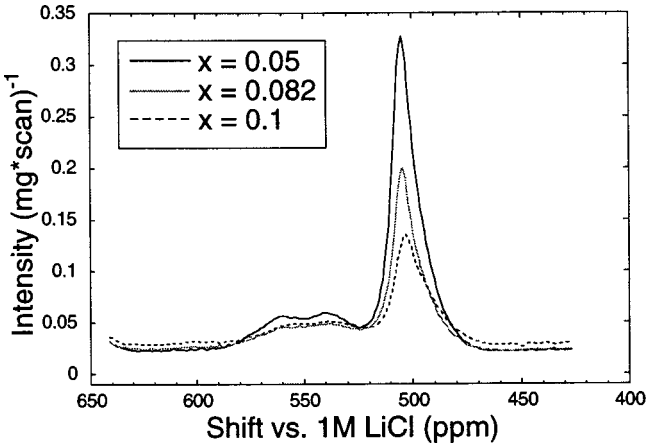

Figure 6. ^{7}Li MAS NMR isotropic tetrahedral peaks for $LiNi_xMn_{2-x}O_4$.

from ~700 ppm (λ-MnO_2)[1] through ~500 ppm ($LiMn_2O_4$)[1,3] to ~100 ppm ($Li_2Mn_2O_4$)[2,3] as the manganese oxidation state is reduced and the e_g orbital is filled.

For all compositions studied, substitution of other metals for manganese resulted in substantial changes in the NMR spectra. In general, substitution leads to a broadening of the peak arising from normal lithium, an increase in the intensity of the peaks arising from near-defect lithium, and small shifts of all observed peaks. In addition to the broadening of the normal lithium peak, a small shoulder on this peak appears to lower shift in the case of Al-, Zn-, and Ni-substitution, and higher shift in the case of Li-, Co-, and Cr-substitution. The linewidth of the peak arising from normal lithium is shown in Fig. 11. For all metal substituents, the linewidth is seen to generally increase with manganese oxidation state. Under MAS, the isotropic peak linewidths are dominated by chemical shift dispersion, so we surmise that increased substitution leads to a greater variety of local environments for the normal tetrahedral lithium as a result of perturbed bond angles and lengths and second nearest neighbor effects. The greatest increase in linewidth is seen for the trivalent cation substituents (Al, Co, Cr) because the number density of substituents required to produce a given manganese oxidation state increases as the substituent oxidation state nears the manganese oxidation state (~3.5) (see Table I). Furthermore, within groups of substituents with like oxidation state, the extent of line broadening increases with substituent ion size. It is interesting to note that the effects of substitution are not localized, but affect the local environment of normal lithium ions, which are spatially removed from the

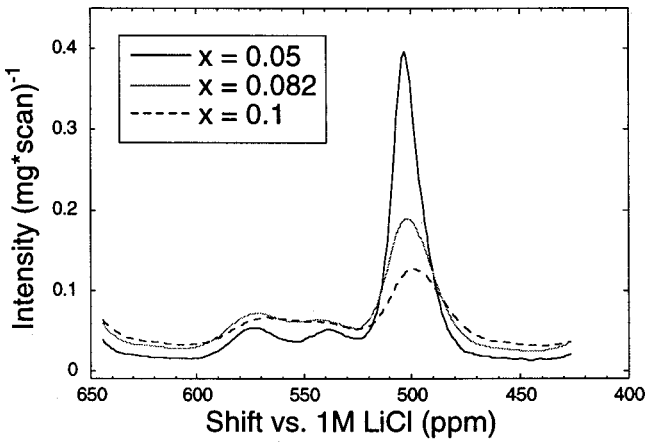

Figure 7. ^{7}Li MAS NMR isotropic tetrahedral peaks for $LiZn_xMn_{2-x}O_4$.

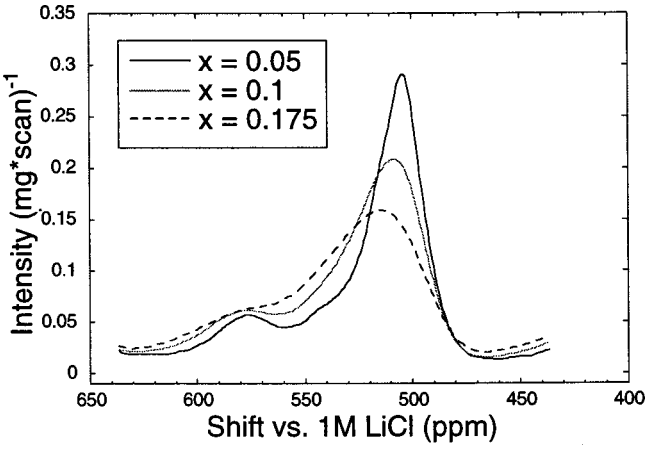

Figure 8. ^{7}Li MAS NMR isotropic tetrahedral peaks for $LiCr_xMn_{2-x}O_4$.

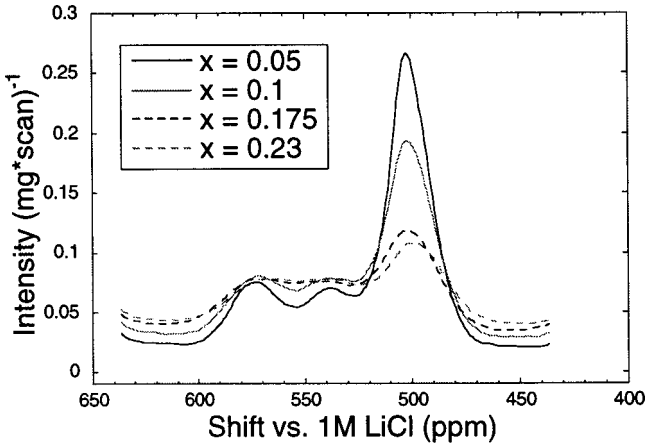

Figure 10. ^{7}Li MAS NMR isotropic tetrahedral peaks for $LiAl_xMn_{2-x}O_4$.

substituting cation. This observation suggests that substitution affects bonding throughout the spinel network, not just in the vicinity of the substituent.

Accompanying the broadening of the normal lithium peak upon substitution is an increase in the intensity of the near-defect lithium peak. In this case, the substituting metal represents a defect in the manganese lattice. As the level of substitution increases, more tetrahedral lithium have fewer than the normal 12 manganese in their coordination spheres, as the manganese is replaced by the substituting cations. Substitution by a cation with oxidation state lower than the average manganese oxidation state requires the local manganese oxidation state in the vicinity of the substituent to increase due to charge neutrality restrictions. This is manifest in a higher shift for those tetrahedral lithium in the vicinity of the substituent. For small levels of substitution, the local manganese oxidation state far from the substituent is expected to remain close to 3.5+. Thus, the shift of the normal lithium peak changes only slightly with substitution. For substitutions resulting in average manganese oxidation states less than 3.6+, the normal tetrahedral peak moves to lower shift by only a few parts per million with increased substitution. Contrarily, in the case of Cr-substitution, the shift of both the normal and near-defect lithium peaks increase with substitution level. Because Cr^{3+} and Mn^{4+} are isoelectronic, substitution by Cr^{3+} increases the unpaired t_{2g} electron density relative to substitution with other cations, effecting an overall increase in the Mn^{4+} electron character and concomitant increase in the lithium chemical shift. In fact, the highest-frequency near-defect peak displays the highest shifts (575-580 ppm) in the Cr-substituted spinels. We rationalize this by postulating that Cr-substitution decreases local unpaired e_g electron density without decreasing local unpaired t_{2g} electron density, unlike the other substituents studied. In contrast, the highest-frequency near-defect peaks with the lowest shifts (555-560 ppm) are observed in the Ni-substituted spinels. Like Cr-substitution, the local manganese oxidation state is still increased in the case of Ni-substitution, but the Ni^{2+} ion has a full (diamagnetic) t_{2g} band and introduces unpaired e_g electron density. All other substituent cations studied here are diamagnetic, and the shifts for the near-defect peaks fall between the extremes presented by the Ni- and Cr-substituted spinels.

Figure 12 shows the first moment of the isotropic peaks arising from tetrahedral lithium as a function of manganese oxidation state. It is clear that for gross changes in the manganese oxidation state, the center of gravity increases, consistent with removal of e_g electrons from the system. For small changes in oxidation state, this gross trend is not necessarily followed. In fact, only the Cr-substituted compounds show this increasing trend without exception, for reasons discussed above. For low levels of substitution by other metals, the first moment of the shift does not vary in a mono-

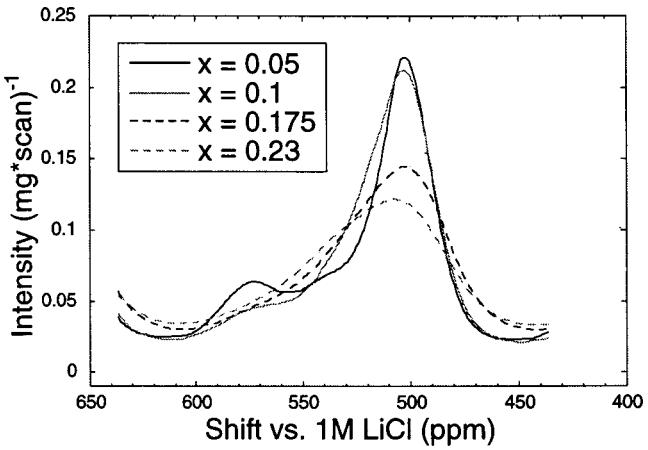

Figure 9. ^{7}Li MAS NMR isotropic tetrahedral peaks for $LiCo_xMn_{2-x}O_4$.

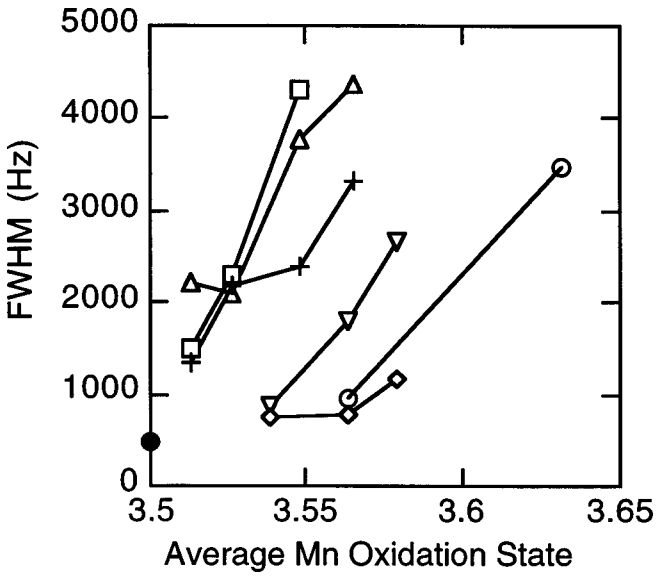

Figure 11. ^{7}Li MAS NMR full width at half-maximum linewidth for the isotropic normal tetrahedral lithium peak of various spinels, $LiM_xMn_{2-x}O_4$. The substituting metals are labeled as (●) $LiMn_2O_4$ (○) Li, (▽) Zn, (◇) Ni, (□) Cr, (△) Co, and (+) Al.

Table I. Inventory of samples organized by metal substituent, M and substitution level, *x*. Average manganese oxidation state is calculated, and electrochemical data for selected compositions is shown.

M	*x*	Mn oxidation state	First discharge capacity (mAh/g)	Capacity retained after 50 cycles (%)
Li^{+}	0	3.500	110	45
Li^{+}	0.05	3.564	114	73
Li^{+}	0.1	3.632	97	95
Li^{+}	0.175	3.740		
Li^{+}	0.25	3.857		
Ni^{2+}	0.05	3.538	112	56
Ni^{2+}	0.082	3.564	108	88
Ni^{2+}	0.1	3.579		
Zn^{2+}	0.05	3.538	112	60
Zn^{2+}	0.082	3.564		
Zn^{2+}	0.1	3.579		
Co^{3+}	0.05	3.513	110	77
Co^{3+}	0.1	3.526	106	85
Co^{3+}	0.175	3.548		
Co^{3+}	0.23	3.565		
Cr^{3+}	0.05	3.513	116	81
Cr^{3+}	0.1	3.526	114	83
Cr^{3+}	0.175	3.548		
Al^{3+}	0.05	3.513	116	64
Al^{3+}	0.1	3.526	110	65
Al^{3+}	0.175	3.548		
Al^{3+}	0.23	3.565		

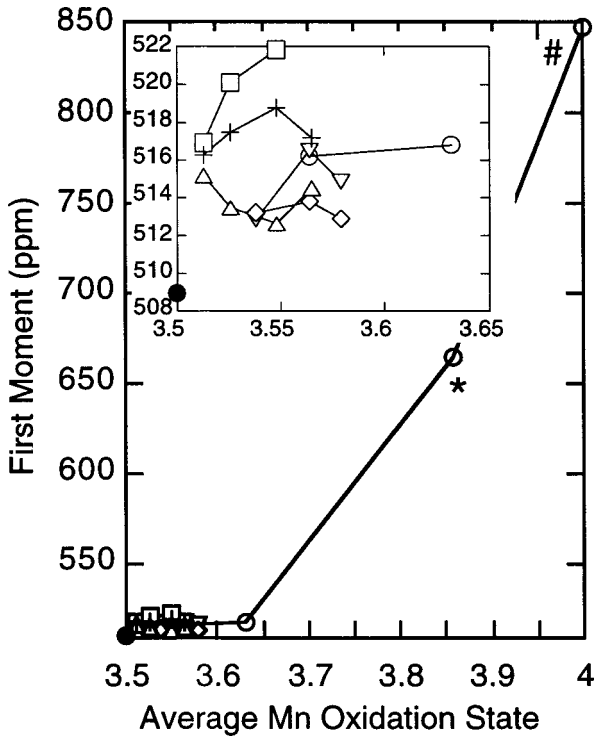

Figure 12. First moment of the chemical shift for the isotropic tetrahedral lithium peaks of various spinels, $LiM_xMn_{2-x}O_4$. The substituting metals are labeled as (●) $LiMn_2O_4$ (○) Li, (▽) Zn, (◇) Ni, (□) Cr, (△) Co, and (+) Al. The point labeled with a (*) was estimated from gaussian fits to the two isotropic peaks shown in Fig. 4e. The point labeled with a (#) was estimated as the isotropic shift value taken from Ref. 3.

tonic fashion. This may be due to competition between the effect of increasing manganese oxidation state and effects arising from the individual substituents such as changes in local bond angles, bond distances, and electronic structure. We must be careful not to infer too much from these trends, as the first moment of the shift does not change by more than a few parts per million over the range of manganese oxidation states probed by the nonlithium substituents, and errors may have been introduced into the calculation of the center of gravity because of overlap of spinning side bands with the edge of the isotropic peaks.

In addition to the major resonances, some spectra show a small resonance in the vicinity of 2052-2059 ppm (Fig. 4e, 5a). Similar resonances have been observed previously[3] in the case of highly lithium-substituted spinels, and were assigned to substitutional lithium in the octahedral 16d site. This peak is clearly visible in the ^{7}Li MAS NMR spectrum for $LiCo_{0.23}Mn_{1.77}O_4$ (Fig. 5a). Similar, but smaller peaks were observed for all Co- and Al-substituted samples with the substitution level $x \geqslant 0.1$. No such peaks were observed for Ni-, Zn-, or Cr-substitution. These observations indicate that displacement of tetrahedral (8a) lithium to octahedral (16d) sites can occur even at low levels of metal substitution for particular cation substituents. It is not yet clear why this effect occurs only for certain metal substitutents. In the case of lithium substitution ($Li_{1+x}Mn_{2-x}O_4$), we expect the full substitutional amount of lithium, *x*, to occupy the 16d site. Only the most highly lithium-substituted sample, $Li_{1.25}Mn_{1.75}O_4$, displayed a peak arising from octahedral lithium, at 2056 ppm. the intensity of this peak, while larger than the similar peaks seen for other metal substituents, was much smaller than the peaks arising from tetrahedral sites in the $Li_{1.25}Mn_{1.75}O_4$ material. Similar results were seen in the case of ^{6}Li MAS NMR results for $Li_{1.33}Mn_{1.67}O_4$.[3] Agreement of our XRD results with those found in the literature for $Li_{1+x}Mn_{2-x}O_4$ [5] does seem to indicate that the intended degree of substitution was achieved. It is not clear why the expected intensity for the octahedral lithium is not observed.

The shift for the peak arising from 16d lithium is almost identical for all samples in which it is observed. This is intriguing, given the wide range of average manganese oxidation states represented by these samples (3.526 for $LiCo_{0.1}Mn_{1.9}O_4$, 3.857 for $Li_{1.25}Mn_{1.75}O_4$). The highly lithium-substituted samples clearly show that the tetrahedral lithium peak shift increases greatly with increasing manganese oxidation state, presumably due to the removal of the negative shift contribution from the Li-Mn^{3+} (e_g electron) interaction as the manganese oxidation state approaches 4+. Unlike the tetrahedral site or the 16c octahedral site, the 16d octahedral site is surrounded by only 90° Li-O-Mn bonds. The manganese e_g orbitals cannot transfer electron spin density to the lithium s orbitals in this arrangement due to geometric reasons.[3] Therefore, the presence or lack of e_g (Mn^{3+}) character is not expected to affect the amount of paramagnetic electron density at the 16d lithium nucleus, and thus, the shift is not expected to change substantially with Mn oxidation state,

Table II. Number of unpaired electrons in the valence shell of all metal substituents.

Metal ion	Unpaired t_{2g} electrons	Unpaired e_g electrons
Mn^{4+}	3	0
Mn^{3+}	3	1
Cr^{3+}	3	0
Co^{3+}	0	0
Al^{3+}	0	0
Ni^{2+}	0	2
Zn^{2+}	0	0
Li^{+}	0	0

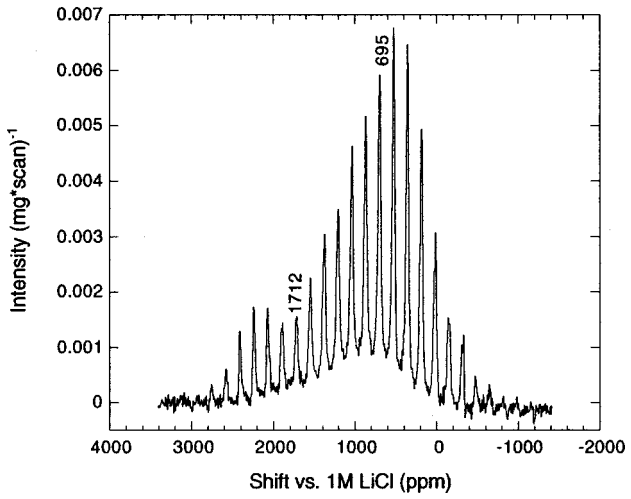

Figure 13. ^{7}Li MAS NMR spectrum of $LiCo_{0.23}Mn_{1.77}O_4$ after electrochemical charging to 4.4 V *vs.* Li/Li^+. Isotropic peaks are labeled.

consistent with the assignment of the peak at ~2050 ppm to 16d octahedral lithium. Finally, an electrode of $LiCo_{0.23}Mn_{1.77}O_4$ composition was charged to 4.4 V in order to remove all electrochemically active lithium; the NMR spectrum of this charged electrode is shown in Fig. 13. The peak arising from 16d octahedral lithium remains after charging, indicating that it is electrochemically inactive lithium, as expected. Some intensity arising from tetrahedral lithium remains after charging, though the peak has shifted to almost 700 ppm due to the increased manganese oxidation state. We surmise that this peak arises from lithium which has been pinned near the cobalt ions to maintain charge neutrality, as suggested by Gao *et al.*[7]

Cycle-life testing.—Selected spinel compositions were cycled electrochemically on the 4 V plateau. Typical discharge curves for several of the materials are shown in Fig. 14. $LiMn_2O_4$ shows the expected electrochemical behavior, with a high utilization and characteristic potential step at 4.1 V. The substituted spinels also show expected behavior, with a smoothing of the potential curve and reduction of the first-discharge capacity relative to the unsubstituted spinel. First-discharge capacity for selected spinels is shown in Table I, and Fig. 15 shows cycle life results for the first 60 cycles of selected spinel compositions. Some of the capacity fade can be attributed to buildup of electrode resistance, as the ohmic recovery at end-of-charge tended to increase with cycle number. However, the clear and reproducible difference between fade rate for different compositions establishes that the majority of the capacity fade is due to changes in the spinel itself. As a representative indicator of fade rate, we show the percent of first-cycle capacity remaining after 50 cycles in Table I. It is clear that substitution greatly increases the cycle life of the spinel. High initial capacity combined with favorable capacity retention was achieved for several Cr-, Ni-, and Li-substituted samples.

NMR results for cycled materials.—After cycling, the spinel electrodes were recovered from the cells and studied with the same NMR techniques used for the as-prepared spinels. XRD analysis of the cycled spinels confirmed bulk retention of the cubic spinel phase, with slightly broadened diffraction peaks after cycling. Figure 16 shows the NMR spectrum for $LiMn_2O_4$ cycled 100 times. Note that no new peaks are introduced after cycling. Figure 17 compares the isotropic tetrahedral peaks for selected as-prepared spinels before and after electrochemical cycling. No electrolyte is detected in the washed electrodes, as any lithium salt would give rise to a sharp peak at 0 ppm. It is clear that the NMR spectra change systematically after cycling. The normal lithium peak is broadened and

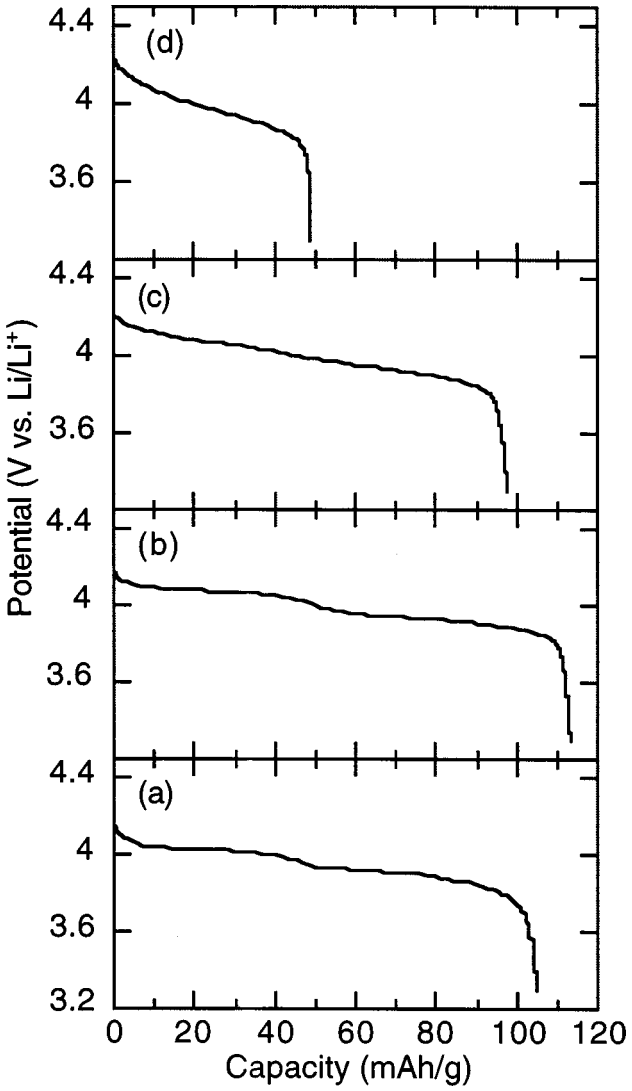

Figure 14. Third cycle discharge profiles for (a) $LiMn_2O_4$, (b) $LiCr_{0.05}Mn_{1.95}O_4$, (c) $Li_{1.1}Mn_{1.9}O_4$, and (d) $Li_{1.25}Mn_{1.75}O_4$.

decreases in intensity, whereas the near-defect peaks are also broadened, but increase in intensity. The changes are observed after even one cycle, and become appreciably more pronounced after 100 cycles, suggesting an evolution of the local spinel structure. This structural evolution is most apparent for $LiMn_2O_4$, which showed the worst capacity fade, and least dramatic for $LiCr_{0.05}Mn_{1.95}O_4$, which showed the best performance of the spinels shown. We surmise, then, that understanding the origin of the NMR-observable changes will elucidate the mechanism of capacity fade in metal-substituted spinels, and the role of metal substitution in capacity stabilization. It should be noted that analogous cycling on the 3 V plateau did not result in any significant changes in the NMR spectra, even though the cycling resulted in a significant capacity fade.[2] This suggests that capacity fade on the 4 V plateau is dominated by local structural changes in the spinel, whereas the spinel retains its structure when cycled on the 3 V plateau where the capacity fade is dominated by changes in particle or bulk electrode characteristics. Furthermore, no new NMR peaks are observed after 4 V cycling, implying that cycling promotes changes in the local environment of lithium in the spinel, but does not destroy the spinel structure or create new phases. We are currently working toward a complete

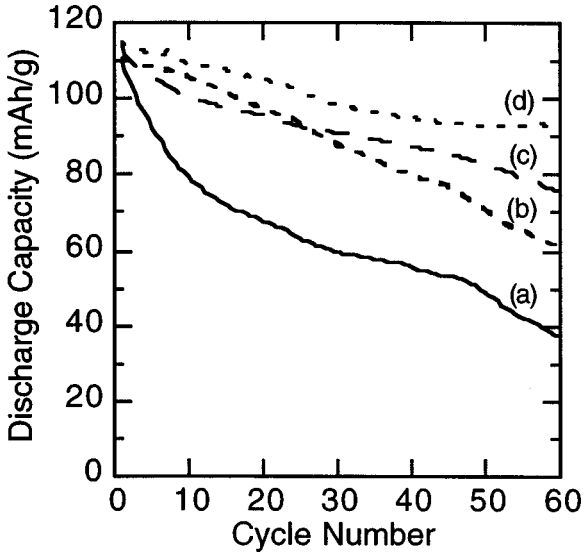

Figure 15. Initial capacity fade for (a) $LiMn_2O_4$, (b) $Li_{1.05}Mn_{1.95}O_4$, (c) $LiAl_{0.1}Mn_{1.9}O_4$, and (d) $LiCr_{0.05}Mn_{1.95}O_4$.

interpretation of the causes of the changes observed in the NMR spectra of cycled materials, which will be the subject of a future publication.

Moisture-induced damage.—The careful exclusion of moisture is well known to be critical for the proper functioning of lithium batteries using liquid electrolytes, especially those with $LiPF_6$ salt. Trace moisture in the cell will react with the electrolyte salt to produce HF, which can cause manganese disproportionation and dissolution at the spinel surface.[8] The products of moisture-related damage are manganese in solution, lithium organic and inorganic surface-electrolyte interface (SEI) byproducts, and delithiated/oxidized manganese oxide.[9] Because we cycle assembled cells outside of a glove box, we undertook a brief study to see if the effects of moisture damage would be observable in the NMR spectra of cycled electrodes if they were not in fact hermetically sealed. Dried $LiMn_2O_4$ electrodes were soaked for two weeks in a small amount of dry electrolyte and electrolyte which had been exposed to atmospheric humidity for a few minutes, hereafter referred to as moist electrolyte. A pink coloration to the supernatant electrolyte indicated that manganese had dissolved from the spinel during storage. XRD analysis of the electrode after storage indicated the cubic spinel phase was still intact, though the lattice parameter had decreased, consistent with a removal of lithium from the spinel.

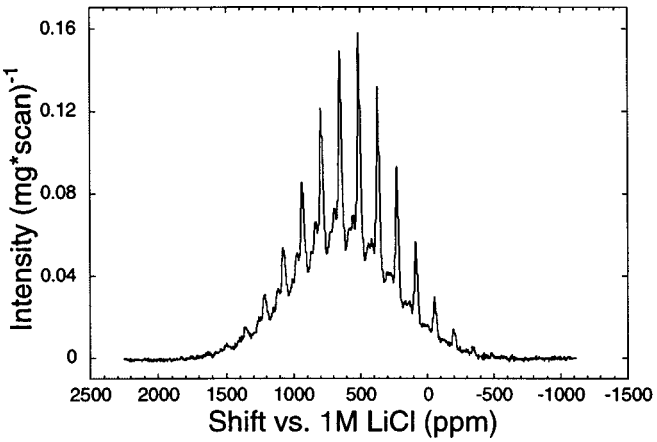

Figure 16. ^7Li MAS NMR spectrum for $LiMn_2O_4$ cycled 100 times.

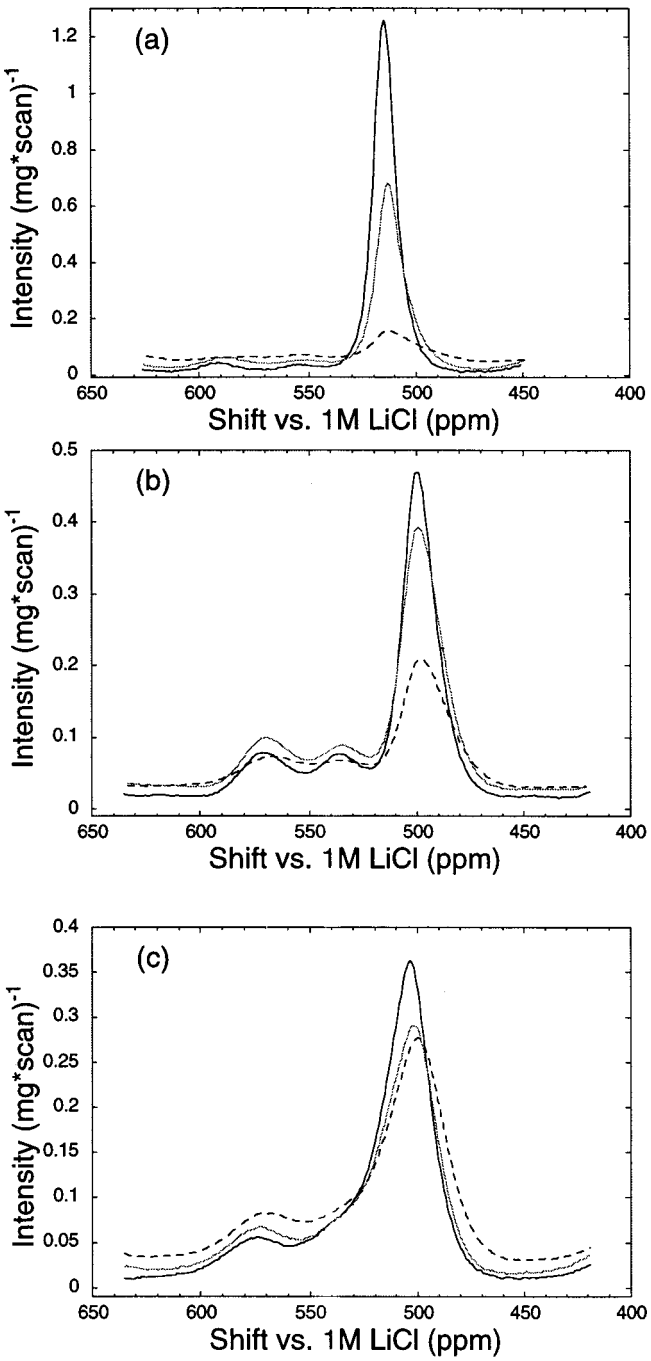

Figure 17. ^7Li MAS NMR isotropic peaks for (a) $LiMn_2O_4$, (b) $Li_{1.05}Mn_{1.95}O_4$, and (c) $LiCr_{0.05}Mn_{1.95}O_4$ before and after cycling. As-prepared: solid black, cycled once: solid gray, cycled 100 times: dashed black.

After storage the electrodes were washed with acetonitrile and studied with the same NMR techniques used for the as-prepared spinels. NMR spectra comparing as-prepared $LiMn_2O_4$, and $LiMn_2O_4$ electrodes soaked in dry and moist electrolyte are shown in Fig. 18. Little change is observed in the NMR spectrum after soaking the electrode in dry electrolyte. In contrast, significant changes are observed for the electrode soaked in moist electrolyte. The lithium NMR intensity is greatly reduced (note Intensity axis scale), the normal lithium peak has disappeared, and new isotropic

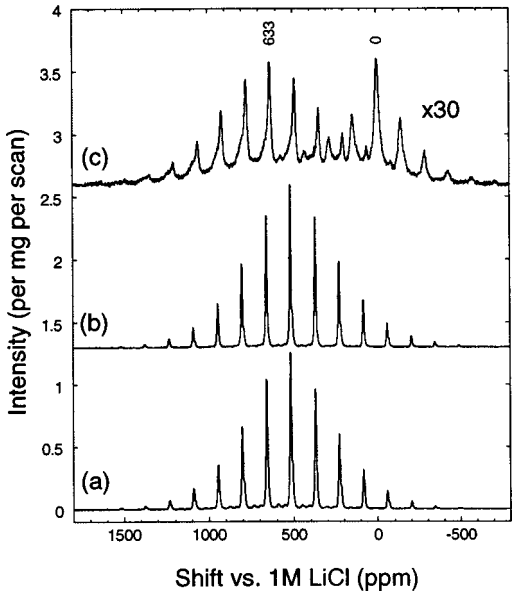

Figure 18. ^{7}Li MAS NMR spectra of $LiMn_2O_4$, (a) as prepared, (b) soaked 2 weeks in dry electrolyte, and (c) soaked 2 weeks in moisture-contaminated electrolyte. Note that (c) is enlarged for clarity.

peaks at 0 ppm and 633 ppm are observed. The spin-lattice relaxation time for the peak at 633 ppm was determined to be a few milliseconds; this time constant is typical of lithium in the spinel, and this fact along with the magnitude of the peak shift leads us to assign the 633 ppm peak to the remaining tetrahedral lithium in a spinel with manganese oxidation state considerably greater than 3.5+ due to manganese disproportionation and lithium extraction. The peak at 0 ppm displayed biexponential spin-lattice relaxation behavior, with characteristic times of about 80 and 200 ms. The 0 ppm peak is, therefore, assigned to a multicomponent SEI layer consisting of diamagnetic lithium species, such as organic electrolyte decomposition products or inorganic lithium salts. The 0 ppm peak is associated with a wide side band manifold, indicating homogeneous broadening. This likely arises from magnetic susceptibility broadening due to proximity of the SEI to the paramagnetic spinel particles. After washing the moisture-damaged electrode with cold water, only about half of the original intensity at 0 ppm remained. No intensity at 0 ppm remained after further washing the electrode with hot water. This supports the assignment of the peak to multiple species. The chemical shift range for lithium in diamagnetic species is so small that it is unlikely that separate peaks arising from the individual SEI components can be distinguished on the basis of chemical shift at our field strength. Moisture-induced damage produces a distinct NMR signature: a reduction in intensity and large shift of the normal lithium peak to higher frequency coupled with the appearance of a new peak at 0 ppm. We conclude that infiltration of moisture was not a contributor to capacity fade in this study, as none of the electrochemically cycled electrodes showed this signature.

Conclusions

We have synthesized a variety of metal-substituted $LiM_xMn_{2-x}O_4$ spinels by traditional solid-state methods, and characterized them with XRD, electrochemical methods and ^{7}Li MAS NMR. ^{7}Li MAS NMR has proved to be a sensitive technique, allowing observation of distinct peaks arising from several types of lattice and nonlattice lithium. In particular, all spinel compositions studied give rise to characteristic peaks in the vicinity of 510 ppm, assigned to normal lithium in a tetrahedral site surrounded by 12 manganese nearest-neighbors, and 530-580 ppm, assigned to near-defect lithium in a tetrahedral site with one or more metal substituents as nearest-neighbors. Upon substitution, the peak arising from normal lithium broadens, and reduces in intensity, while the peaks arising from near-defect lithium increase in intensity. In addition to these peaks, Li-, Co-, and Al-substituted spinels also give rise to a peak in the vicinity of 2050 ppm, assigned to electrochemically inactive lithium in the 16d octahedral site. Spinels damaged by the presence of moisture in the electrolyte show a reduction in intensity and shift of the peak arising from tetrahedral lithium in the spinel, as well as a peak at 0 ppm arising from diamagnetic SEI species. No signs of moisture damage were observed for spinels cycled in sealed cells. All substituted compounds displayed better capacity retention than $LiMn_2O_4$, with some Cr-substituted spinels showing a quite high initial capacity and favorable capacity retention. Cycling on the 4 V plateau introduces notable changes in the NMR spectrum of the spinels, including broadening and reduction in intensity of the normal lithium peak, and an increase in the intensity of the near-defect lithium peaks. The extent of these changes was greatest for those spinels that displayed poor cycling behavior. Future work will focus on systematic interpretation of the changes observed in the spinel structure after cycling.

Acknowledgments

This work was supported by the National Science Foundation through a fellowship for M.C.T., and by the Director, Office of Basic Energy Sciences, Chemical Sciences Division of the U.S. Department of Energy, under contract DE-AC03-76SF00098.

University of California at Berkeley, and the Lawrence Berkeley National Laboratory assisted in meeting the publication costs of this article.

References

1. B. Gee, C. R. Horne, E. J. Cairns, and J. A. Reimer, *J. Phys. Chem. B,* **102**, 10142 (1998).
2. M. C. Tucker, J. A. Reimer, and E. J. Cairns, *Electrochem. Solid-State Lett.,* **3**, 463 (2000).
3. Y. J. Lee, F. Wang, and C. P. Grey, *J. Am. Chem. Soc.,* **120**, 12601 (1998).
4. Y. J. Lee, F. Wang, S. Mukerjee, J. McBreen, and C. P. Grey, *J. Electrochem. Soc.,* **147**, 803 (2000).
5. Y. Gao and J. R. Dahn, *J. Electrochem. Soc.,* **143**, 1783 (1996).
6. R. D. Shannon, *Acta Crystallogr., Sect. A: Cryst. Phys., Diffr., Theor. Gen. Crystallogr.,* **32**, 751 (1976).
7. Y. Gao, J. N. Reimers, and J. R. Dahn, *Phys. Rev. B,* **54**, 3878 (1996).
8. Y. Xia, Y. Zhou, and M. Yoshio, *J. Electrochem. Soc.,* **144**, 2593 (1997).
9. J. C. Hunter, *J. Solid State Chem.,* **39**, 142 (1981).